Lattice-dynamical and ground-state properties of CaF_2 studied by inelastic neutron scattering and density-functional methods

K. Schmalzl,[1,2,*] D. Strauch,[1,†] and H. Schober[2,‡]
[1]*Institut für Theoretische Physik, Universität Regensburg, D-93040 Regensburg, Germany*
[2]*Institut Laue-Langevin, F-38042 Grenoble Cedex 9, France*
(Received 5 March 2003; revised manuscript received 21 July 2003; published 17 October 2003)

We report results on the lattice dynamics of the superionic conductor CaF_2 from experiment and theory. Coherent inelastic neutron scattering between room temperature and 1000 °C gives an unusually large temperature dependence of the phonon frequencies (dispersion) and widths. Electronic and lattice-dynamical properties are obtained from *ab initio* density-functional theory employing pseudopotentials and plane-wave basis sets, the electronic properties also from full-potential linearized augmented plane waves–linearized muffin-tin orbital methods. From density-functional perturbation theory we have calculated the dispersion of the phonon frequencies and of the mode-Grüneisen parameters. The contribution from thermal expansion to the experimental line shift is separated from the other anharmonic (phonon-phonon) contributions by comparison with the theoretical line shift from the volume expansion. The temperature dependence of the line broadening can in most cases be rationalized in terms of the two-phonon combined density of states, but the width of the zone-boundary X_2' mode is unexpectedly large, even though the two-phonon combined density of states shows that there are only few two-phonon decay channels, and the frequency becomes critically soft at higher volumes. The effective charges and the dielectric constant depend nonlinearly on volume.

DOI: 10.1103/PhysRevB.68.144301 PACS number(s): 61.12.Ex, 61.50.Ah, 63.20.Dj, 63.20.Ry

I. INTRODUCTION

Calcium fluoride (CaF_2) crystallizes in the (fluorite) fcc structure with three atoms in the unit cell. The crystal volume can be viewed as being composed of tetrahedra and octahedra with the Ca^{2+} ions at the corners and the F^- ions at the centers of the tetrahedra, see Fig. 1.

Ionic conductors are promising candidates for solid-state electrolytes to be used in batteries. CaF_2 is a prototype ionic conductor showing a strong increase of the conductivity with temperature that saturates at 1420 K,[1] where it becomes comparable to that of a molten salt; the melting temperature is near 1690 K.[1,2] Despite considerable efforts, the origin of the ionic transport is not completely clarified in CaF_2. Motional disorder in the fluorine sublattice, hopping over potential barriers, and the formation of various types of defects are certainly essential ingredients for ionic conduction.[3] Details of the conduction mechanism, however, depend on peculiarities of the structure and dynamics as demonstrated by a comparison with other ionic conductors, e.g., LaF_3.

In order to add to the general understanding of ionic conduction we have investigated the static and dynamic lattice properties of CaF_2 both theoretically by means of *ab initio* calculations as well as experimentally by coherent inelastic neutron scattering. As the process of ionic conduction involves hopping over potential barriers, ionic motion is an intrinsically anharmonic and strongly temperature-dependent process. Even at temperatures below the onset of ionic conductivity, the ions will experience the anharmonic potential. We have thus focused on the thermal motion of the atoms by investigating the temperature and volume dependence of the lattice dynamics.[4]

Experimentally, the temperature dependence of the modes seems to be unknown except for the optic vibrations at the Brillouin-zone (BZ) center, which have been investigated by Raman scattering[5,6] and infrared-reflection and -absorption spectroscopy.[7,8] The anharmonic potential has also been probed in pressure infrared,[8,9] Raman,[10–12] and ultrasound[13] experiments.

An unusually strong temperature dependence of the lowest-frequency (longitudinal) X_2' mode on the BZ boundary has been claimed repeatedly in the literature,[14–16] but we have not been able to find an original experimental report.

Previous theoretical work[17–20] has been based on phenomenological potentials leading to quantitatively somewhat unreliable results. Also calculations using semiempirical potentials[15,21] may possibly not properly account for the effects of electronic redistribution during the formation of defects.

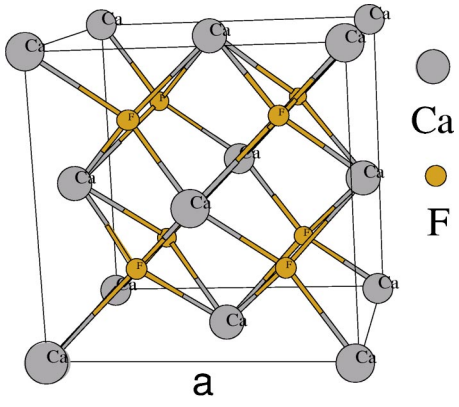

FIG. 1. Crystal structure of CaF_2. The cube contains four formula units; a complete octahedron is spanned by the Ca^{2+} ions on the face centers of the cube, while a tetrahedron is spanned by a Ca^{2+} ion on a cube corner and the three Ca^{2+} ions on the adjacent face centers.

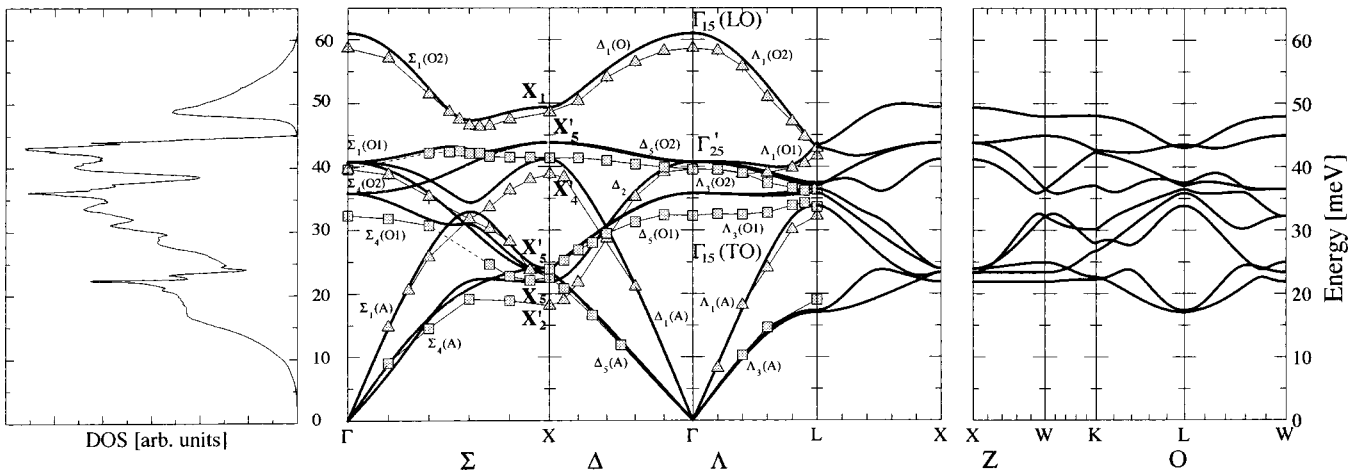

FIG. 2. CaF_2. Middle and right: Phonon-dispersion curves from inelastic neutron scattering (data points with thin connecting lines) at RT and from *ab initio* theory (lines), see Sec. III C below. Triangles refer to longitudinal, and squares to transverse polarization. The three curves along the Σ direction without labels (second, fifth, and sixth curve from bottom to top) indicate the modes invisible in the scattering geometry of our experiment. Left: Phonon density of states from *ab initio* theory.

Our paper is structured as follows. The experimental results on the wave vector and temperature dependence of the phonon frequencies and widths are reported in Sec. II. In Sec. III we present theoretical results for the ground-state, dynamical, and volume-dependent properties. In Sec. IV we summarize our results.

II. INELASTIC NEUTRON SCATTERING

A. Experimental setup

The coherent inelastic neutron-scattering experiments have been performed on the instruments IN3 (preliminary) and (mostly) IN1 at the high-flux neutron reactor of the Institut Laue-Langevin in Grenoble (France). The size of the single crystal was approximately $25\times25\times25$ mm^3.[22] The sample, oriented with the $[1\bar{1}0]$ axis perpendicular to the scattering plane, was mounted in a furnace heated to 300, 673, 873, 1073, and 1273 K.

For the experimental runs on IN3, a Cu(111) monochromator and a horizontally curved PG(002) analyzer have been used with open collimation; for the setup on IN1 we have employed a Cu(220) monochromator and a Cu(200) analyzer with a relaxed collimation of 25′-60′-60′-60′ and, for the refinement of some room-temperature (RT) data, with a tighter collimation of 25′-30′-30′-30′. The spectra have been taken in the fixed k_F mode with $k_F=3.0$ Å^{-1} on IN3 and with $k_F=5.0$ Å^{-1} and $k_F=4.1$ Å^{-1} on IN1. The calculated instrumental resolution on IN1 varied between approximately 3.5 and 6.8 meV for the different energy and momentum transfers.

B. Phonon-dispersion curves

With three atoms per unit cell one obtains nine phonon branches (six along [001] and [111] due to the degeneracy of the transverse branches). The orientation of the crystal makes the scattering to take place in the $(1\bar{1}0)$ plane, which allows the observation of all phonon branches along the main-symmetry directions [001] (Δ), [111] (Λ), and [110] (Σ), except the three branches along Σ with phonon polarization vectors perpendicular to the scattering plane. Our experimental data at RT are shown in Fig. 2 (middle panel). They compare well with those of Ref. 23 which, however, are not only somewhat scarce in the higher-energy regime but also carry sizable error bars.

The experiments have been accompanied by *ab initio* calculations, see Sec. III C below. Due to their reliability, these *ab initio* results assist in assigning the symmetry to the various phonon-dispersion branches. Since phonons with the same wave number can be observed for momentum transfer from different Brillouin zones, the *a priori* calculation of the scattering intensities from the theoretical phonon eigenfrequencies and eigenvectors can be (and has been) used to select the zone with the highest scattering intensity for a given phonon. Also, the theoretical scattering intensities can be (and have been) used to unravel badly resolved bands.

C. Anharmonic phonon frequency shift and width

Fits have been done via a convolution of the damped harmonic oscillator function with the calculated Gaussian instrumental resolution. All spectral lines shift and become unusually broad with increasing temperature; some examples of raw experimental data are shown in Figs. 3 and 4. The anharmonic shift and width of the phonon frequencies along the Δ and Λ directions are shown in Figs. 5 and 6. At higher temperatures, the widths of the phonon peaks become comparable to the frequencies themselves, see also Figs. 7 and 8 below.[24]

There are various ways to show the temperature dependence of the frequency shift. Rather than $d\omega_\lambda/dT$ or something similar, we have chosen to plot

$$\tilde{\gamma}_\lambda = -\frac{dT}{d\ln V}\frac{d\ln\omega_\lambda}{dT} = -\frac{1}{3\alpha_T}\frac{d\ln\omega_\lambda}{dT} \qquad (1)$$

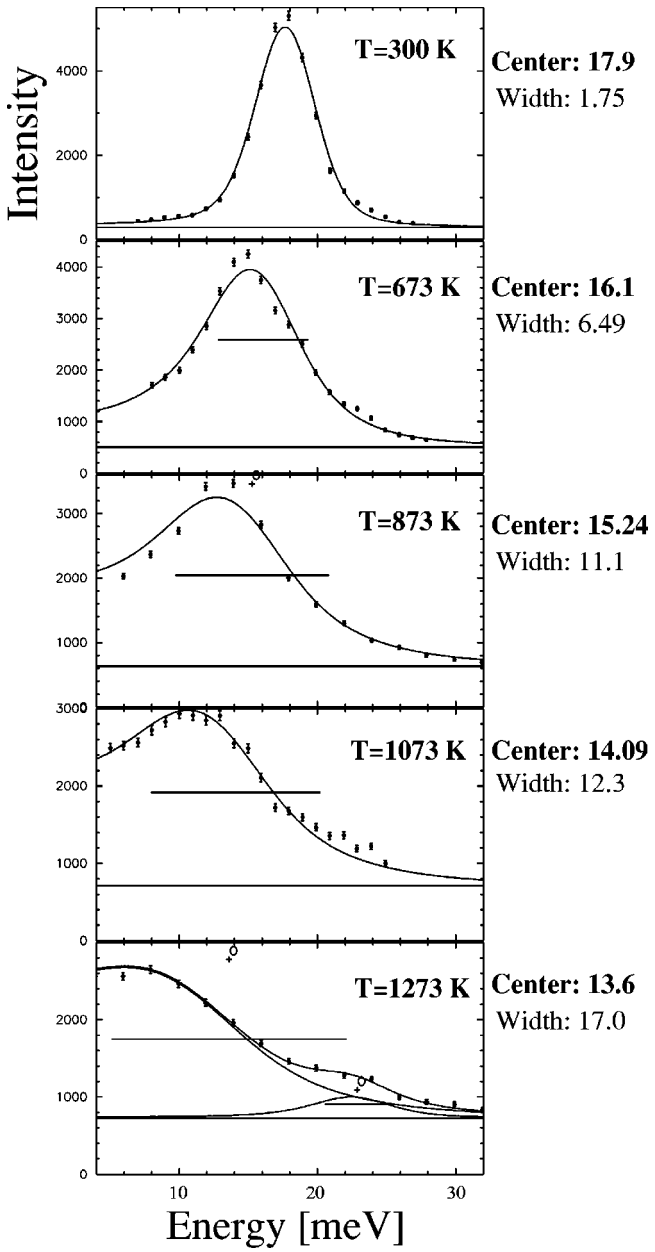

FIG. 3. Phonon excitations in CaF_2: Experimental raw data (points) from inelastic neutron scattering measured at $\mathbf{Q}=(6,1,1)\times(2\pi/a)$ and damped-harmonic-oscillator plus constant-background fits (lines) for the lowest-frequency X_2' mode at the X point of the zone boundary. The horizontal bar indicates the width of the oscillator with the (harmonic) frequency at its center. Numerical results of the fits are given to the right of the figures. The band evolving at high temperatures near 20 meV of unknown origin is possibly multiphonon background, since the contribution of the difference processes with resulting wave vector from the X point has a contribution to the two-phonon density of states near this frequency, see Fig. 14 below.

in Fig. 5 with the coefficient of linear thermal expansion,[25] $\alpha_T=28.4\times10^{-6}$ K^{-1} at 700 K. This choice has been made for the sake of later comparison with the theoretical contribution from the volume expansion in Sec. III E below. The data carry appreciable (but otherwise undetermined) error bars since the spectral bands are unusually broad and are contaminated by multiphonon background and (in particular at long waves) by strong (quasi)elastic scattering.

Comparison with other experimental data for CaF_2 can be made only for the modes at the Γ point; a more detailed discussion is deferred to Sec. III E, where values of $\tilde{\gamma}_{\mathrm{Raman}}\approx1.2$, $\tilde{\gamma}_{\mathrm{TO}}\approx2.3$, and $\tilde{\gamma}_{\mathrm{LO}}\approx0.35$ are derived.

To fully appreciate the observed anharmonic properties, it should be recalled that phonon linewidths normally remain significantly smaller than the respective frequencies up to the melting point. For example, among the alkali halides LiF (with a TO frequency comparable to that of CaF_2) has the largest TO mode width which is about one-third of the TO frequency at 1060 K; in MgO the ratio is less than one-tenth;[26] in Si, which has a melting point similar to CaF_2, the width of the Γ_{25}' Raman mode at a frequency of 61.75 meV is 1.74 meV at 1140 K.[27] At present, we do not have an explanation for the fact that the width of the Γ_{25}' Raman mode (our data are shown in Fig. 8) is more than twice of that extracted from Raman experiments.[5,6]

Since the ionic conductivity in CaF_2 is caused by the motion of the F^- ions, we have turned our particular attention to those modes in which the F^- ions have the largest vibrational amplitudes. These are (i) the modes in which the Ca^{2+} ions are at rest, namely, the X_1 ($E=\hbar\omega\approx48$ meV) and X_2' mode ($E\approx18$ meV) at the X point on the Brillouin-zone boundary; actually, the Ca atoms are at rest for the entire Δ_2 branch that starts at 40 meV at the Brillouin-zone center and ends at 18 meV at the X point. Among these modes, (ii) the ones with the smallest frequencies have the largest amplitudes.

We have found an anomaly in the temperature dependence of the (lowest-frequency) X_2' mode in that this mode shows a decrease in frequency with increasing temperature, which is much larger than that of all the other modes, as shown in Figs. 3, 5, and 7. While the broadening of this line is at first sight not as conspicuous as the shift, even though it is the largest at the X point, see Figs. 6 and 8, the theoretical considerations in Sec. III F below will show that it equally has to be considered as exceptional.

III. THEORETICAL RESULTS

A. Theoretical methods *ab initio*

The electronic and ground-state (lattice-static) properties have been determined using density-functional methods, and the lattice-dynamical properties have been determined from density-functional perturbation theory (response theory). We have employed the method of full-potential linearized augmented plane waves (FP-LAPW) plus local orbitals (using the WIEN97 code[28]) and the pseudopotential method (using the ABINIT[29] and VASP[30] codes). The pseudopotential calculations have been done with Hartwigsen-Goedecker-Hutter (HGH) pseudopotentials[31] (within ABINIT) and with ultrasoft pseudopotentials[32] (within VASP). The comparison with the full-potential method shows the reliability of the pseudopotential methods, the VASP code being fast because of the use of ultrasoft pseudopotentials.

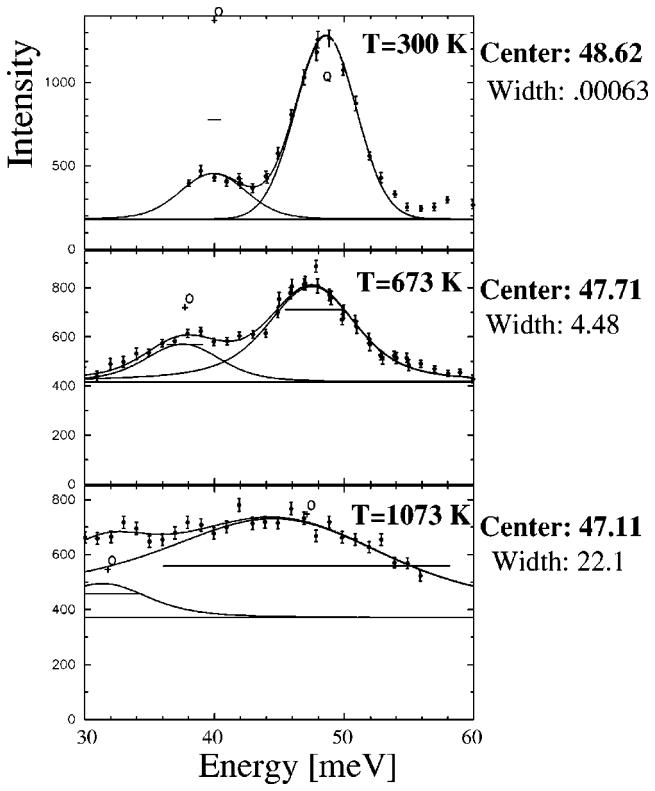

FIG. 4. Same as Fig. 3, but for the high-frequency X_1 mode (and the upper X_4' mode on the low-energy shoulder) measured at $\mathbf{Q}=(7,0,0)(2\pi/a)$.

The local-density approximation (LDA) and the generalized gradient approximation (GGA) in the form of Refs. 33 (PW) and 34 (PBE) have been used and their respective merits investigated, in particular, for the influence on the lattice constant as the important part of the static properties and the key quantity for the succeeding calculation of the dynamical properties.

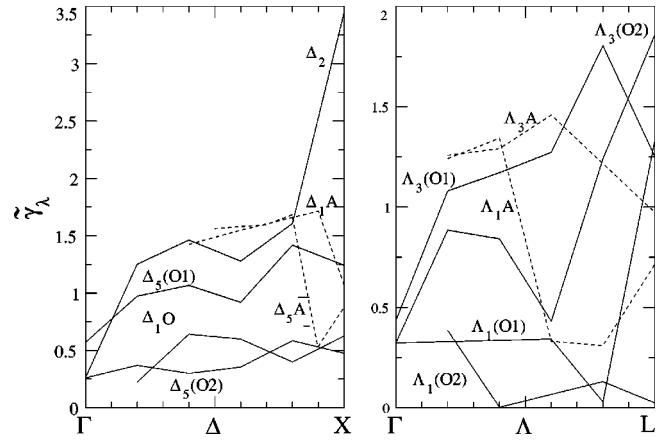

FIG. 5. Experimental wave-vector dependence of the anharmonic relative phonon frequency shift according to Eq. (1) obtained by fitting a straight line to the temperature dependence of $\ln\omega_\lambda$. The labels of the branches are the same as those of the dispersion curves in Fig. 2.

B. Static properties: Ground state and lattice constant

A precise determination of the ground-state properties is needed as a starting point for the investigation of the dynamical properties. In the ABINIT code, typical values of 100 Ha for the cutoff energy and a $4\times4\times4$ Monkhorst-Pack **k**-vector mesh have been sufficient for a relative precision of 10^{-3} for the ground-state energy, see Fig. 9. For the VASP code, the cutoff energy of around 40 Ha has been needed. The FP-LAPW calculations have been performed with muffin-tin radii of 1.8 a.u. for Ca and F. The wave functions have been expanded up to a maximum value of $l_{\max}=10$ for the angular momentum quantum number, and a cutoff energy of 25 Ry has been used.

The electronic band structure is shown in Fig. 10 and the corresponding density of states (DOS) in Fig. 11. The band structure has a conduction-band minimum at the Γ point and a valence-band maximum at the *X* point with the gap energies listed in Table I. As a typical result of the LDA and GGA, the gap between the valence- and conduction-state energies is much smaller than the experimental excitation gap energy [12.1 eV from far-UV reflectivity[35] and 11.2 eV for electron-hole excitations (excitons)[35,36]]. A calculation[37] within the GW approximation gives 11.38 eV. The electronic band structure[38] from the method of first-principles orthogonalized linear combination of atomic orbitals (OLCAO) with LDA differs in detail and gives an indirect gap of 6.53 eV [8.20 eV with self-interaction correction (SIC)]. Different Hartree-Fock calculations[37,39] result in quite different gap energies; an LCAO calculation[40] with Slater exchange gives an indirect band gap of 9.8 eV; a similar calculation[41] for the valence band combined with an OPW calculation for the conduction band gives too large a gap which can be brought down to the experimental value by reducing the Slater exchange parameter. The form of the band structure of Ref. 40 is disputed[42] on the grounds of spectroscopic ellipsometry experiments. With the help of the theoretical difference between direct- and indirect-gap energies, an experimental gap energy of 11.8 eV is estimated in Ref. 35.

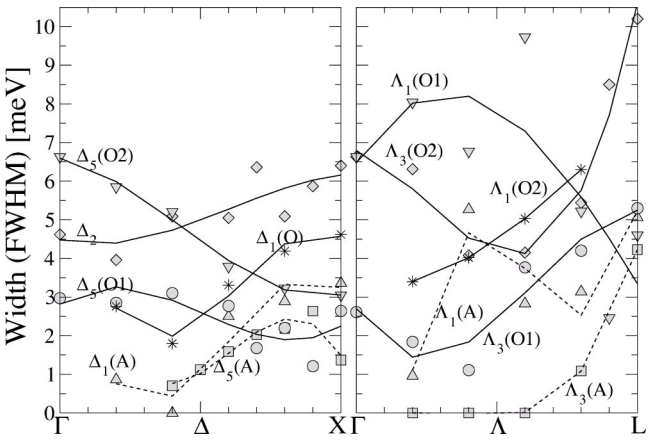

FIG. 6. Experimental wave-vector dependence of the anharmonic phonon width at 673 K. Lines are guides to the eye. The labels of the branches are the same as those of the dispersion curves in Fig. 2.

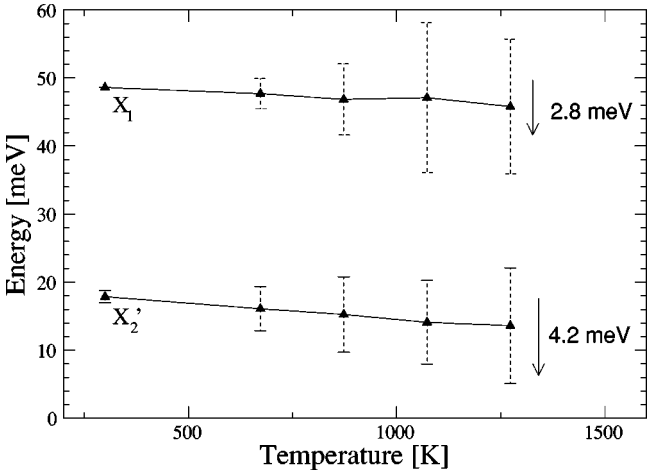

FIG. 7. Highest and lowest *X*-point mode frequencies vs temperature; the vertical bars indicate the width (as shown in more detail in Fig. 8) of the measured phonon peak at the *X* point on the Brillouin-zone boundary.

While our DOS is essentially identical to the one calculated in Ref. 43 using the same method, the gap-energy value of 7.8 eV from the FP-LAPW method (WIEN code with GGA) as given in Ref. 43 seems to be a misprint, since the density of states in that paper definitely exhibits contributions at smaller values. (Note that the conduction-band DOS is very low below around 8 eV, such that from the DOS the gap may appear larger than from the band structure.)

As is commonly done, we have determined the theoretical lattice constant from the (numerical) minimum of the total energy (rather than from the free energy) using the above-mentioned first-principles techniques. Like in other cases, the LDA underestimates the value of the lattice constant, and the GGA overestimates it, see Table II. Table II also shows that the results for the lattice constant from the WIEN97 and ABINIT codes are essentially identical and that those from the VASP code are systematically smaller. Since the effect of the zero-point fluctuations on the thermal expansion is not negligible even at room temperature (the maximum phonon frequency corresponds to more than twice the room temperature), the harmonic lattice constant must be appreciably lower than the experimental RT value; extrapolating from high (900 K) to low temperatures assuming linear thermal expansion[25] at higher T gives $a \approx 5.35$ Å, to which the theoretical values should be compared.

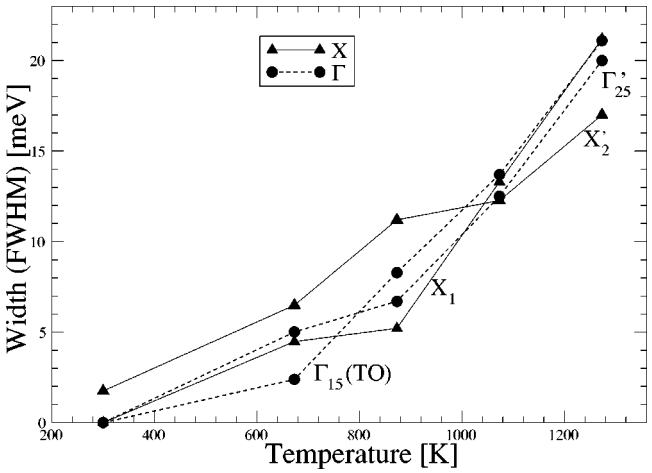

FIG. 8. FWHM of selected phonon excitations at the Γ and *X* points vs temperature.

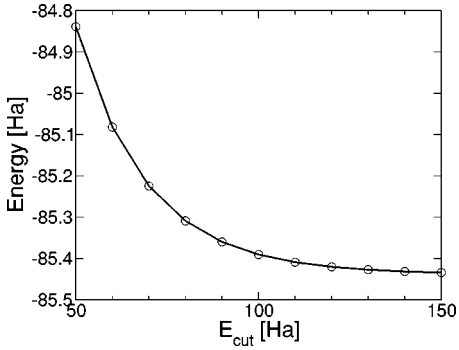

FIG. 9. Ground-state energy vs energy cutoff from the ABINIT code.

Because of the high cutoff energy of 100 Ha needed for the HGH pseudopotential of the Ca atom (as also found in Ref. 44), the use of a (new) Troullier-Martins (TM) pseudopotential[45] is reported in Ref. 44, which needs a cutoff energy only half as large and which renders less accurate results for the dielectric properties. Using the CRYSTAL code, results[46] range from the input in Table II to $a = 5.519$ from density-functional-theory (DFT) calculations with still another exchange-correlation functional and $a = 5.532$ from Hartree-Fock calculations.

C. Dynamical properties: Lattice dynamics

The dynamical properties have been calculated with the theoretical lattice constant as the input. The underestimation (overestimation) of the value of the lattice constant within the LDA (GGA) generally leads to an overestimation (underestimation) of the frequencies, see Table III.

Macroscopic electric fields are essential in the case of CaF_2 as they become apparent in the large LO-TO splitting, see Table III and also Sec. III G below. Since the ABINIT code, in contrast to the other ones, allows for the inclusion of macroscopic electric fields, this code has been used for the further investigation of the dynamical properties.

Figure 2 shows the results of the *ab initio* calculation (together with our neutron data) of the phonon-dispersion curves for CaF_2 in several directions together with the one-phonon density of states. When comparing the theoretical with the experimental dispersion curves, one has to keep in mind that the theoretical results are strictly harmonic and that the experimental data are taken at RT and thus contain (strong) anharmonic contributions. In particular, the theoretical lattice constant is smaller than the experimental one resulting in larger theoretical frequencies. Since the anharmonic effects are weak at low temperatures, a low-temperature experiment would be desirable for a comparison. Anyway, using the experimental instead of the

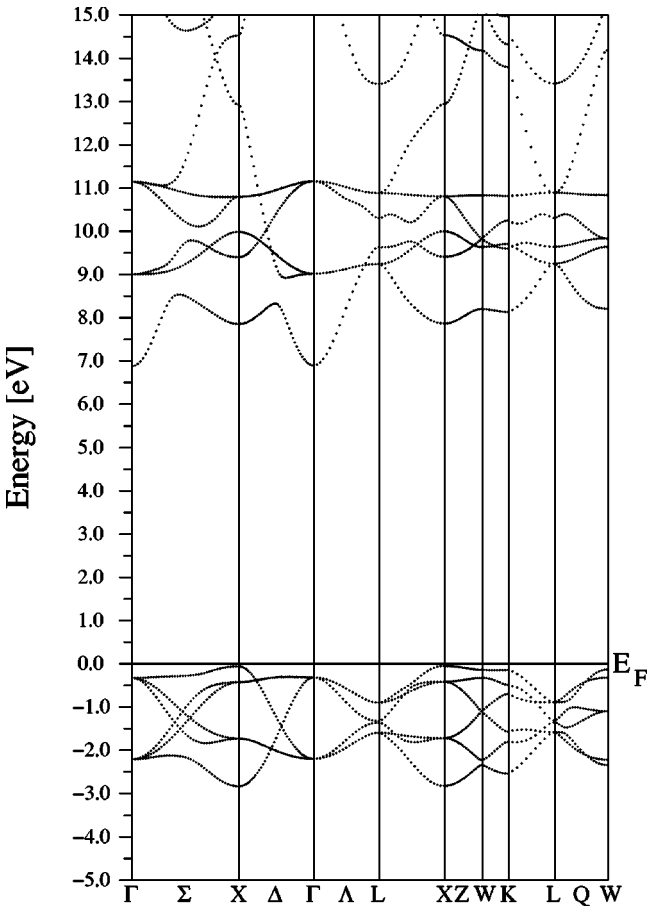

FIG. 10. Electron band structure of the highest occupied and lowest unoccupied states from the FP-LAPW (WIEN97) calculation using LDA. The Fermi energy has been chosen as $E_F=0$ at the top of the valence bands. See Fig. 11 for the corresponding density of states.

theoretical lattice constant in the calculations results in frequencies which are generally smaller than the experimental ones.

We will discuss the temperature dependence of the experimental and thus anharmonic dispersion curves in more detail in Sec. III E below.

D. Anharmonic phonon self-energy

The anharmonic line shift and linewidth can be determined from the real and imaginary part of the phonon self-energy, respectively. To leading order of perturbation theory, there are three processes contributing to the self-energy. These are (1) the two-phonon decay process, (2) the coupling to thermal fluctuations, and (3) the process of thermal expansion. All three processes contribute to the line shift, but only the first (decay) process (1) contributes to the linewidth.[48,49]

At sufficiently high temperatures the contributions of all three processes are linear in temperature; higher-order processes result in a dependence upon higher powers of the temperature.

To the best of our knowledge, the only (anharmonic) density-functional response calculation of the complete dispersion of the anharmonic linewidth is the one of Ref. 50 (for Si and Ge). Other density response calculations of the anharmonic linewidth[51] and shift[52] have been restricted so far to the $\mathbf{q}=0$ mode as well as to diatomic semiconductors. (Due to the importance of macroscopic electric fields, molecular-dynamics calculations do not seem to be the appropriate approach in the case of CaF_2.) The calculation of the anharmonic coupling constants for the present system and for arbitrary wave vectors poses a true challenge. While such calculations would shed light on our experimental findings, they are numerically involved in the case of CaF_2 and are far beyond the scope of the present paper.

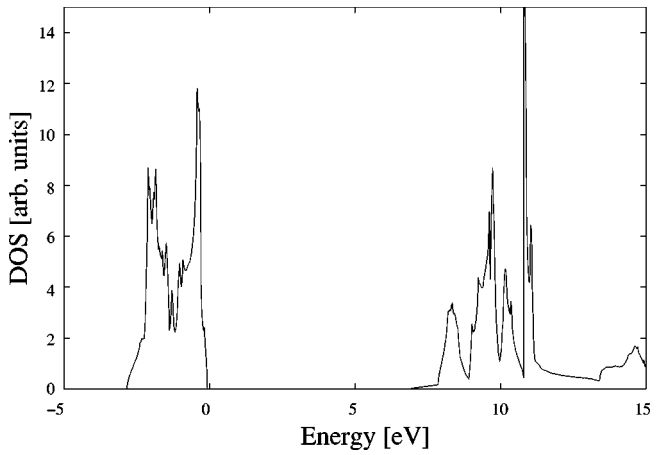

FIG. 11. Electron density of the highest occupied and lowest unoccupied states from the FP-LAPW (WIEN97) calculation using LDA. See Fig. 10 for the corresponding band structure.

E. Volume dependence of phonon frequencies and mode-Grüneisen parameters

Process (3) of thermal expansion can be investigated with *ab initio* methods without recourse to the anharmonic coupling constants or lowest-order perturbation theory.

Dispersion curves have been calculated for various volumes. To first order in perturbation theory, the shift of the square of the phonon frequency is proportional to the change of the lattice constant. This dependence is given by the mode-Grüneisen parameters

$$\gamma_\lambda = -\frac{d\ln\omega_\lambda}{d\ln V} = -\frac{1}{6}\frac{d\ln\omega_\lambda^2}{d\ln a}.$$

TABLE I. Energies (in eV) of the direct and indirect gap as obtained with the WIEN97 code. Calculations are performed within LDA and GGA (PBE). Lattice constants a are taken either from the minimization of the total energy (a_{theor}) or from experiment (a_{expt}), see Table II.

	Indirect-gap energy		Direct-gap energy	
	(a_{expt})	(a_{theor})	(a_{expt})	(a_{theor})
LDA	6.95	7.38	7.21	7.66
GGA (PBE)	7.34	7.24	7.59	7.49

TABLE II. Comparison of the calculated lattice constants a (in Å) with the experimental value.

Method	LDA	GGA (PW)	GGA (PBE)
WIEN97 [a]	5.333	5.482	5.493
VASP [a]	5.173	5.44	
ABINIT (HGH) [a]	5.33		
ABINIT (TM) [b]	5.352		5.564
CRYSTAL [c]	5.346	5.513	
Expt. (Extrapolated) [d]	5.35		
Expt. (300 K) [e]	5.463		

[a]This work.
[b]Reference 44 with TM pseudopotential.
[c]Reference 46.
[d]See text.
[e]Reference 47.

Figure 12 shows the theoretical volume dependence of the squared mode frequencies at the X and Γ point of the Brillouin zone over a larger range of lattice constants. Thermal-expansion data[25] have been used to convert the temperature dependence of our experimental results to a volume dependence.

The close-to-linear dependence of ω^2 on a [as required for process (3)] within the experimentally accessible range of lattice constants is confirmed by Fig. 12. The deviation of the theoretical results from straight lines is due to higher-order anharmonic terms, i.e., the mode-Grüneisen parameters themselves depend on volume. These corrections become most obvious in the highest-frequency X_1 mode. The $\omega^2(a)$ dependence for this mode shows variations not only in the slope but even in the sign of the curvature.

The fact that the LDA underestimates the experimental lattice constant by about 0.13 Å (see Table II) leads to a horizontal offset of the theoretical against the experimental curves. Taking this offset into account, the theoretical and experimental frequency shifts agree very well at lower temperatures (smaller lattice constants). While the slope of the theoretical and experimental curves in Fig. 12 generally agree for the modes at the X point, this is not so for the modes at the Γ point. We are, therefore, led to the conclusion that most of the anharmonic contributions for the modes at the X point can be described via the effect of thermal expansion and that the contributions of other anharmonic processes are either weak or nearly cancel for the X-point modes but that these processes are important for the Γ-point modes, at least at higher temperatures.

TABLE III. Comparison of calculated Γ-point energies in meV with experimental values.

	Expt. (300 K)	LDA	WIEN97 GGA (PBE)	GGA (PW)	ABINIT LDA
Γ_{15} (TO)	32.28	34.58	29.61	29.99	34.67
deviation (%)		7.1	−8.3	−7.1	7.4
Γ'_{25} (Raman)	39.6	41.89	38.09	38.42	41.66
deviation (%)		5.8	−3.8	−3.0	5.2
Γ_{15} (LO)	58.65				60.33
deviation (%)					2.9

The theoretical mode-Grüneisen parameters (based on the theoretical lattice constant) are given in Fig. 13 for all modes along the [001] (Δ) and [111] (Λ) directions. Shell-model-type calculations[53] result in very similar results, if only the O1↔O2 labels are interchanged in that work. The results of calculations[54] employing a model potential show very little resemblance.

We now direct our attention to specific modes. Our value of $\gamma_{\mathrm{Raman}}=2.0$ for the Γ'_{25} Raman mode is only slightly larger than the experimental values 1.9,[10] 1.8,[11] and 1.47[12] obtained from pressure experiments. The value of $\tilde{\gamma}_{\mathrm{Raman}}=1.25$ derived from the temperature dependence[5] is much smaller (and our estimate gives a similar value using the data of Ref. 6).

Our value of $\gamma_{\mathrm{TO}}=2.4$ for the Γ_{15} TO mode lies between the experimental values of 3.2 (Ref. 8) and 1.8 (Ref. 9) from pressure experiments; using temperature data[8] we estimate $\tilde{\gamma}_{\mathrm{TO}}=2.3$. From the same data we also estimate $\tilde{\gamma}_{\mathrm{LO}}=0.35$ for the Γ_{15} LO mode as compared to our value of $\gamma_{\mathrm{LO}}=1.15$. Model calculations[55] supply a large range of values, $1.2<\gamma_{\mathrm{TO}}<3.2$ and $0.65<\gamma_{\mathrm{LO}}<1.7$.

For the difference between $\tilde{\gamma}_\lambda$ and γ_λ, the contributions of processes (1) and (2) are invoked, which contribute to $\tilde{\gamma}_\lambda$ but not to γ_λ. A more quantitative statement will have to await future investigations.

For the zone-center acoustic modes in the [001] direction, we find $\gamma_{\mathrm{TA}[001]}=0.75$ for the transverse and $\gamma_{\mathrm{LA}[001]}=1.56$ for the longitudinal modes, where pressure ultrasonic experiments[13] give $\gamma_{\mathrm{TA}[001]}=1.41$ and $\gamma_{\mathrm{LA}[001]}=1.34$. For the [111] direction we find $\gamma_{\mathrm{TA}[111]}=0.64$ for the transverse and $\gamma_{\mathrm{LA}[111]}=1.80$ for the longitudinal mode, in excellent agreement with the experimental results of $\gamma_{\mathrm{TA}[111]}=0.627$ and $\gamma_{\mathrm{LA}[111]}=1.94$.

From the good agreement of the theoretical and experimental mode-Grüneisen parameters at the Brillouin zone center we conclude that our predicted Grüneisen parameters are realistic in the whole of the BZ. On the other hand, we have commented on the experimental error bars in Sec. II C, and the following comparison of the experimental $\tilde{\gamma}_\lambda$ from Fig. 5 to the theoretical γ_λ from Fig. 13 has to be taken with due care. Also, one has to keep in mind that processes (1) and (2) contribute to $\tilde{\gamma}_\lambda$ but not to γ_λ.

The values of $\tilde{\gamma}_\lambda$ and γ_λ span a comparable range, and the sign and magnitude of the slopes of the curves for the optical modes (as a function of wave vector) generally agree, except for the Δ_5(O1) and Λ_3(O1) TO branches where $\tilde{\gamma}_\lambda$ and γ_λ have opposite slopes.

The most obvious difference occurs near the Brillouin-zone center where $\tilde{\gamma}_\lambda$ is generally smaller than γ_λ, indicating an appreciable (positive) net contribution of processes (1) and (2) at longer wavelengths. At the X point the largest difference of $\tilde{\gamma}_\lambda$ and γ_λ occurs for the X'_5 mode on the Δ_5(O2) branch and the X_5 mode on the Δ_5(A) branch.

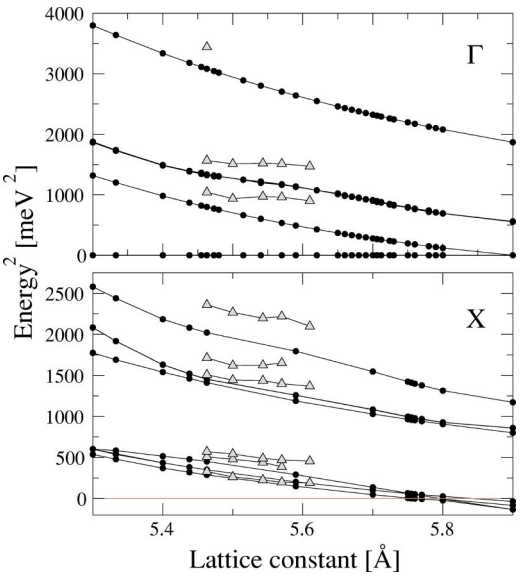

FIG. 12. Theoretical volume dependence of the squared mode frequencies at the X and Γ points (full symbols) in comparison with experimental data (open triangles) showing the consecutive softening of various modes.

Near the L point there is an indication of a particularly strong positive net contribution of processes (1) and (2) to the frequency shift only for the Λ_1(A) branch. The only negative contribution to the shift occurs for the Λ_3(A) branch.

At least for the shorter-wavelength modes the contribution of process (3) dominates the one of the combined processes (1) and (2). In particular, the shift of the X_5' mode on the Δ_5(O1) branch and of the X_2' mode (on the Δ_2 branch) is determined by only the effect of process (3). The latter already stands out in Fig. 5, where the largest shift in frequency with temperature can be found for the lowest-frequency mode at the zone boundary, even though that frequency is only slightly smaller than that of the other two low-frequency modes.

The volume dependence of the lowest-frequency X_2' mode deserves special attention. Already at room temperature the theoretical harmonic frequency differs strongly from the experimental one. From Fig. 13 we conclude that this mode is particularly sensitive to the changes in the lattice constant. With theory underestimating the experimental lattice constant by 3%, a 9% error in the frequency is thus to be expected. For a theoretical lattice constant of $a \approx 5.76$ Å, definitely below melting (at $a \approx 5.8$ Å in our calculation, where the TA elastic constant softens) the X_2'-mode frequency goes to zero, see Fig. 12. (A slightly smaller value of 5.62 Å has been obtained in Ref. 14 from a semiempirical potential.) This critical softening is confined to the immediate neighborhood of the X point.

It has been argued[14–16] that the softening of the X_2' mode is related to the onset of ionic conductivity, since both effects occur at similar temperatures and lattice constants. In this zone-boundary mode entire chains of F^- ions move in the cubic-axis direction with the Ca^{2+} ions at rest. It is apparently of importance that neighboring chains move out of phase. The in-phase motion of such chains (against the Ca^{2+} ions) occurs in the Γ_{15} LO mode; but the frequency of the LO mode is about three times as high as that of the X_2' mode, even though the effective mass of the LO mode is about twice as large.

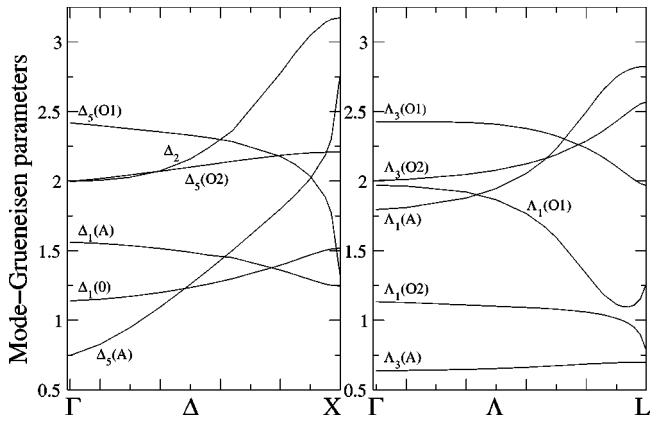

FIG. 13. Theoretical wave-vector dependence of the mode-Grüneisen parameters. The labels of the branches are the same as those of the dispersion curves in Fig. 2.

As a collective phenomenon, the softening of the X_2' mode indicates the instability of the lattice against the formation of a superstructure, which, to our knowledge, has not been observed experimentally, yet. Possibly, the thermal fluctuations may suppress this collective transition but may support the local formation of defect structures necessary for the ionic conductivity.

Disregarding the consequences of the X_2'-mode instability a further homogeneous expansion of the crystal leads to a softening of the transverse acoustic branches Δ_5(A) and Σ_4(A) at long wavelengths, related to the softening of the shear elastic constant c_{44}. This instability may be related to the transition from the crystalline to the liquid state (melting). At still larger volumes we find the softening of the transverse optic mode at the Γ point, which is the type of softening related to a ferroelectric phase transition with a diverging static dielectric constant like in a conducting state.

In any case, our calculations can only give hints for instabilities as a function of volume. In experiments the external control parameters are temperature and pressure. Due to the neglect of other anharmonic effects in the calculation it is impossible to directly translate the theoretical volumes into experimental transition temperatures.

F. Two-phonon density of states and line width

The width of a phonon with quantum number $\lambda_0 \equiv (\mathbf{q}_0, j_0)$ ($\mathbf{q}_0$ is the wave number and j_0 the branch index) and frequency ω_0 is caused by the decay process (the other two processes mentioned in Sec. III D contribute to the shift only). To lowest order of perturbation theory, the corresponding damping function is proportional to[48,49]

$$\Gamma_{\lambda_0}(\omega) \propto \sum_{\lambda_1 \lambda_2} |\Phi(\lambda_0, \lambda_1, \lambda_2)|^2 [(1+n_1+n_2)\,\delta(\omega_1+\omega_2-\omega) + (n_2-n_1)\,\delta(\omega_1-\omega_2-\omega)] \quad (2)$$

for $\omega \geqslant 0$. Here $\Phi(\lambda_0,\lambda_1,\lambda_2)$ is the anharmonic coupling constant. The temperature dependence of $\Gamma_{\lambda_0}(\omega)$ arises from the Bose occupation numbers

$$n_i = [\exp(\hbar\omega_i/k_B T) - 1]^{-1}.$$

Expression (2) for Γ_{λ_0} contains two terms: The first term within the square brackets describes the annihilation of the phonon under consideration (with quantum number λ_0) by simultaneous creation of two other phonons (λ_1 and λ_2) (or vice versa, the so-called summation processes), and the second term describes the annihilation of the phonon (λ_0) together with another one (λ_2) to create a third one (λ_1) (or vice versa, the so-called difference processes). The difference processes have a cutoff energy given by the one-phonon maximum frequency and vanish at lowest temperatures due to $n_i \to 0$ for $T \to 0$. The summation processes have a cutoff energy at twice the maximum phonon frequency.

The phonon damping *constant* is approximately[56,57] given by $\Gamma_{\lambda_0}(\omega_0)$, i.e., the damping *function* taken at the frequency $\omega = \omega_0$.

If, in a rough approximation, the anharmonic coupling constants $\Phi(\lambda_0,\lambda_1,\lambda_2)$ in Eq. (2) are assumed not to depend on the quantum numbers $\lambda_i = (\mathbf{q}_i, j_i)$ except for the quasimomentum conservation, then the phonon width Γ_{λ_0} is proportional to the two-phonon density of states,

$$D_{\mathbf{q}_0}(\omega) = \sum_{\lambda_1\lambda_2} \sum_{\mathbf{G}} \delta_{\mathbf{q}_0,\mathbf{q}_1+\mathbf{q}_2+\mathbf{G}}[(1+n_1+n_2)\delta(\omega_1+\omega_2-\omega) + (n_2-n_1)\delta(\omega_1-\omega_2-\omega)] \quad (3)$$

(here weighted by thermal occupation numbers), shown in Fig. 14. **G** is a reciprocal-lattice vector. $D_{\mathbf{q}_0}(\omega)$ is independent of the branch index j_0, and so is the damping *function* in this approximation, while the damping *constant* $\Gamma_{\lambda_0}(\omega_0) \propto D_{\mathbf{q}_0}(\omega_0)$ does depend on the branch through the frequency ω_0.

We will now analyze the linewidth with the help of expression (3) by starting with the Γ point. Since the two-phonon density of states at the Γ'_{25} Raman-mode frequency is only slightly larger than that of the Γ_{15} TO-mode frequency, see top panel of Fig. 14, the linewidth of the Raman mode should be only slightly larger than that of the TO mode in this approximation. This is indeed observed, see Fig. 8. On the other hand, the width of the Γ_{15} LO mode should be larger than the other two by factors of about 4 and 3 compared to the Γ_{15} TO mode and the Γ'_{25} Raman mode, respectively, in this approximation. In good agreement with this prediction, the experiment at high temperatures gives a factor of 3.7 and 3 for the Γ_{15} TO mode and for the Γ'_{25} Raman mode, respectively.

In the region of the low-frequency X'_2 mode (calculated energy of 21.9 meV) the contribution of the summation processes to the two-phonon density of states vanishes. The reason is that energy and momentum conservation cannot be fulfilled simultaneously (due to the negative curvature of the transverse-acoustic dispersion sheet). Thus, the width of the

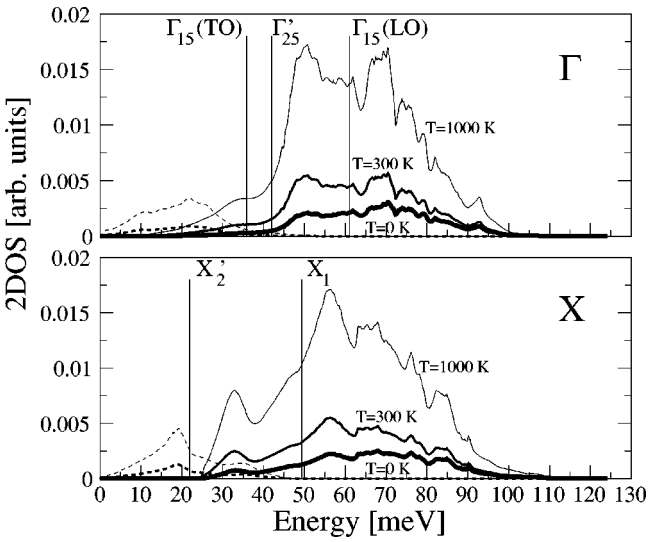

FIG. 14. Weighted two-phonon combined density of states, $D_{\mathbf{q}_0}(\omega)$, of Eq. (3) for phonon wave vector $\mathbf{q}_0$ at the Γ point (top panel) and the X point (bottom panel) for the theoretical equilibrium lattice constant. Shown are the contributions from the summation processes (full lines) and difference processes (broken lines). The vertical bars indicate the position of the frequencies at the Γ point and of the lowest and highest frequencies at the X point, cf. Fig. 2.

X'_2 mode is due to the difference processes only, and this contribution is very low at low temperatures. In other words, there are very few decay channels for the low-frequency modes, and consequently the width should be very much smaller than the one of the higher-frequency modes. While the ratio of the experimental half-widths of the X'_2 and X_1 modes is roughly equal to 1:1, see Fig. 8, the ratio of the theoretical two-phonon densities of states at these two frequencies is rather 1:5 at 300 K and 1:4 at 1000 K, see Fig. 14. This difference indicates a particularly strong anharmonic coupling constant $\Phi(\lambda_0,\lambda_1,\lambda_2)$ for λ_0 denoting the X'_2 mode.

For $k_B T \gg \hbar\omega$ the Bose factors and thus the two-phonon density of states depend linearly on temperature. This is ex-

TABLE IV. Calculated (from DFT) and experimental results for the high-frequency dielectric constant and effective charge.

Method	a (Å)	Z^*	ϵ_∞
ABINIT (HGH) [a]	5.33	2.373	2.378
ABINIT (HGH) [b]	5.46	2.36	2.32
ABINIT (TM-LDA) [b]	5.46	2.18	2.06
ABINIT (TM-GGA) [b]	5.46	2.18	2.03
DFT-GGA [c]	5.464		2.12
OLCAO-LDA [d]	5.46		2.02
OLCAO-LDA (SIC) [d]	5.46		1.80
Expt. (300 K) [e]	5.463		2.045

[a]This work.
[b]Reference 44.
[c]Reference 37.
[d]Orthogonalized linear combination of atomic orbitals, Ref. 38.
[e]Reference 7.

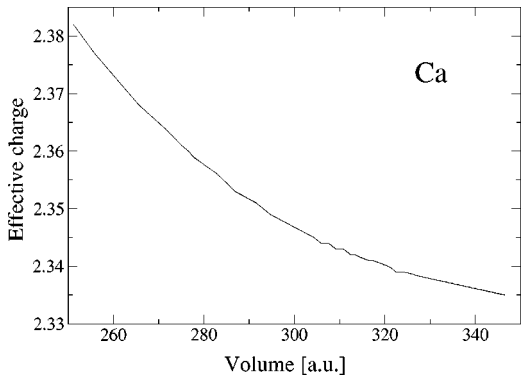

FIG. 15. Theoretical volume dependence of the effective charge Z^*_{Ca} of the Ca^{2+} ion.

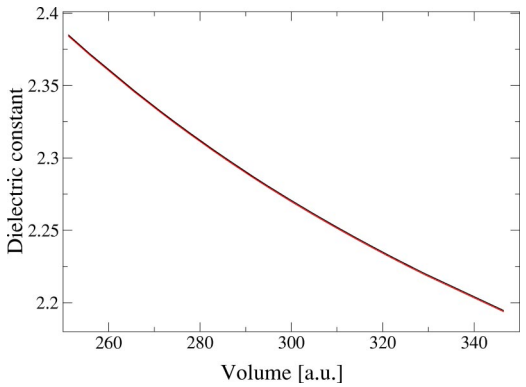

FIG. 16. Theoretical volume dependence of the high-frequency dielectric constant ε_∞.

actly what we observe experimentally for the widths of the phonon excitations above approximately 600 K, see Fig. 8. The temperature dependence of these widths can thus be explained via the two-phonon density of states without the need of higher-order processes.

G. Volume dependence of the high-frequency dielectric constant and of the Born effective charges

At the Γ point there is a threefold degenerate Raman-active mode near 40 meV and three infrared-active modes with a huge LO-TO splitting given by

$$\omega_{\mathrm{LO}}^2-\omega_{\mathrm{TO}}^2=\frac{(Z^*e)^2}{\varepsilon_0\varepsilon_\infty\mu v_0}$$

($\hbar\omega_{\mathrm{LO}}\approx 60$ meV, $\hbar\omega_{\mathrm{TO}}\approx 30$ meV, see Fig. 2), caused by large effective charges with $Z^*=Z^*_{\mathrm{Ca}}=-2Z^*_{\mathrm{F}}$.

Our calculations yield $Z^*=2.373$ at the theoretical ground-state volume of $V=256$ a.u., see Table IV, while the TM potentials give smaller and less accurate values[44] and are at variance with our volume dependence, see Fig. 15. The fact that the effective charge is larger than the nominal ionic charge of $Z_{\mathrm{Ca}}=2$ seems to indicate that there is an electronic antiscreening rather than a screening effect for the Γ_{15} vibrations.

We also find $\varepsilon_\infty=2.378$ at the ground-state volume of 256 a.u., see Table IV; the TM potentials differ, but are in agreement with other DFT calculations.[37,38] A semiempirical bond-orbital calculation[58] gives $\varepsilon_\infty=2.04$. The LDA and GGA values are typically larger than the experimental[7] values.

The results of our calculations exhibit a theoretical volume dependence of the LO-TO splitting, which must be related to the volume dependence of the effective charges and/or of the high-frequency dielectric constant ε_∞. Our *ab initio* results for these volume dependencies are shown in Figs. 15 and 16. In contrast to assumptions generally made in pressure experiments, the volume dependence of the dielectric constant and, even more so, of the effective charges turns out not to be linear, indicating the importance of processes beyond lowest-order perturbation theory for these quantities. At the theoretical equilibrium volume we find $(d\ln|Z^*|)/(d\ln V)\approx 0.10$; from pressure experiments[8] a value of 0.5 is extracted.

IV. CONCLUSIONS

We have studied the static and dynamical lattice properties of the ionic conductor CaF_2 both by experiment and by theory. While various computer codes give similar results for the ground-state properties, they differ in their approach to the lattice dynamics; in particular, the huge LO-TO splitting requires a treatment within the advanced response theory (i.e., density-functional perturbation theory) in which macroscopic electric fields are incorporated.

The inelastic neutron-scattering experiments exhibit a strong dependence of the dynamical properties on temperature, indicating a strong anharmonicity of the interionic potential. This becomes most obvious in the linewidths of the excitations. While in semiconductors the phonons broaden only moderately even close to the melting point and while in other ionic crystals the dynamics remain in an underdamped situation, the phonon widths in CaF_2 become comparable to the frequencies at high temperatures even well below melting. This exceptional broadening is not confined to particular regions in $(\mathbf{q},\omega)$ space, i.e., the high anharmonicity of the interionic potential affects all of the excitations. The temperature dependence of the broadening of various modes is found to scale with the (weighted) two-phonon density of states. This holds apart from the X point region of the Brillouin zone.

Apart from broadening the modes soften with increasing temperature. Both, experimental data and numerical *ab initio* calculations, give large mode-Grüneisen parameters with values of up to more than 3. The general anharmonic mode softening near the Brillouin zone boundaries can be described on the basis of just thermal expansion indicating that the other processes give contributions to the softening that cancel to a large extent, while for decreasingly smaller wave vectors the multiphonon processes give increasing contributions to the frequency shift.

From theory, the lowest-frequency X_2' mode softens critically at higher temperatures, and the analysis of the width and shift suggests a very large anharmonic coupling constant. This mode involves the motion of the F^- ions while

the Ca^{2+} ions are at rest. The critical softening indicates a structural transition with doubling of the unit cell, with an fcc network of Ca^{2+} ions, but with displaced F^- ions. At present, we cannot draw any direct conclusion about the relation of this mode to the onset of ion conduction.

Finally, the high-frequency dielectric constant and the effective charges are calculated to depend nonlinearly on volume.

Future work will have to be directed towards *ab initio* calculations of the anharmonic coupling parameters. From our findings of the nonlinear volume dependencies, processes of higher order than those discussed in Sec. III D will have to be considered.

ACKNOWLEDGMENTS

We gratefully acknowledge the cooperation of M. Letz, who engaged himself in negotiations with Schott Lithotec. We thank F. Fujara for his interest in this investigation. M. Saad, O. Lips, G. Deinzer, and H. Dobler gave a helpful hand with taking the experimental data; G. Deinzer kindly supplied some routines for the calculation of the density of states. M. Verstraete and X. Gonze kindly sent us a preprint of their work.[44] Last but not least, we gratefully acknowledge the continued interest of B. Dorner and A. Ivanov (ILL) in the project and their helpful support; the paper has benefited from their critical reading of the manuscript.

*Electronic address: schmalzl@ill.fr

†Electronic address: dieter.strauch@physik.uni-regensburg.de

‡Electronic address: schober@ill.fr

[1] See the review by J.B. Boyce and B.A. Huberman, Phys. Rep. **51**, 189 (1979).

[2] B.F. Naylor, J. Am. Chem. Soc. **67**, 75 (1945).

[3] M.T. Hutchings, K. Clausen, M.H. Dickens, W. Hayes, J.K. Kjems, P.G. Schnabel, and C. Smith, J. Phys. C **17**, 3903 (1984).

[4] A short and selective account is given by K. Schmalzl, D. Strauch, H. Schober, B. Dorner, and A. Ivanov, *High Performance Computing in Science and Engineering 2002—Transactions of the First Joint HLRB and KONWIHR Result and Reviewing Workshop*, edited by S. Wagner, W. Hanke, A. Bode, and F. Durst (Springer, Berlin, 2003), p. 243; K. Schmalzl, D. Strauch, and H. Schober, Physica B (to be published).

[5] D.G. Mead and G.R. Wilkinson, J. Phys. C **10**, 1063 (1977).

[6] R.J. Elliott, W. Hayes, W.G. Kleppmann, A.J. Rushworth, and J.F. Ryan, Proc. R. Soc. London, Ser. A **360**, 317 (1978).

[7] W. Kaiser, W.G. Spitzer, R.H. Kaiser, and L.E. Howarth, Phys. Rev. **127**, 1950 (1962).

[8] R.P. Lowndes, J. Phys. C **4**, 3083 (1971).

[9] J.R. Ferraro, H. Horan, and A. Quattrochi, J. Chem. Phys. **55**, 664 (1971).

[10] S.S. Mitra (unpublished, data cited in Ref. 9).

[11] J.K. Kessler, E. Monberg, and M. Nicol, J. Chem. Phys. **60**, 5057 (1974).

[12] G.A. Kourouklis and E. Anastassakis, Phys. Status Solidi B **152**, 89 (1989).

[13] C. Wong and D.E. Schuele, J. Phys. Chem. Solids **28**, 1225 (1967).

[14] L.L. Boyer, Phys. Rev. Lett. **45**, 1858 (1980).

[15] L.L. Boyer, Solid State Ionics **5**, 581 (1981).

[16] See, e.g., L.X. Zhou, J.R. Hardy, and H.Z. Cao, Solid State Commun. **98**, 341 (1996).

[17] A. Rahman, J. Chem. Phys. **65**, 4845 (1976).

[18] M.J. Gillan, J. Phys. C **19**, 3391 (1986).

[19] G.A. Evangelakis and V. Pontikis, Phys. Rev. B **43**, 3180 (1991).

[20] P.J.D. Lindan and M.J. Gillan, J. Phys.: Condens. Matter **3**, 3929 (1991); **5**, 1019 (1993).

[21] N.T. Wilson, M. Wilson, P.A. Madden, and N.C. Pyper, J. Chem. Phys. **105**, 11 209 (1996).

[22] The crystal was kindly supplied by Schott Lithotec.

[23] M.M. Elcombe and A.W. Pryor, J. Phys. C **3**, 492 (1970).

[24] The overdamping of the X_2' mode was found also in empirical-potential molecular-dynamics simulations of the scattering function at (2,1,1) in Ref. 18.

[25] A.S. Touloukian, R.K. Kirby, R.E. Taylor, and T.Y.R. Lee, *Thermal Expansion—Nonmetallic Solids*, Thermophysical Properties of Matter Vol. 13 (IFI/Plenum, New York/Washington, 1977). The literature values for thermal expansion agree very favorably with the temperature dependence of the lattice constants measured in our INS experiments.

[26] J.R. Jasperse, A. Kahan, J.N. Plendl, and S.S. Mitra, Phys. Rev. **146**, 526 (1966).

[27] M. Balkanski, R.F. Wallis, and E. Haro, Phys. Rev. B **28**, 1928 (1983).

[28] P. Blaha, K. Schwarz, P. Sorantin, and S.B. Trickey, Comput. Phys. Commun. **59**, 399 (1990); see http://www.tuwien.ac.at/theochem/wien97/

[29] X. Gonze, Phys. Rev. B **55**, 10 337 (1997); see http://www.abinit.org/

[30] G. Kresse and J. Furthmüller, Phys. Rev. B **54**, 11 169 (1996); see http://tph.tuwien.ac.at/vasp/

[31] C. Hartwigsen, S. Goedecker, and J. Hutter, Phys. Rev. B **58**, 3641 (1998).

[32] G. Kresse and J. Hafner, J. Phys.: Condens. Matter **6**, 8245 (1994).

[33] J.P. Perdew and Y. Wang, Phys. Rev. B **45**, 13 244 (1992).

[34] J.P. Perdew, K. Burke, and M. Ernzerhof, Phys. Rev. Lett. **77**, 3865 (1996).

[35] G.W. Rubloff, Phys. Rev. B **5**, 662 (1972).

[36] G. Stephan, Y. Le Calvez, J.C. Lemonier, and S. Robin, J. Phys. Chem. Solids **30**, 601 (1969).

[37] E.L. Shirley, Phys. Rev. B **58**, 9579 (1998).

[38] F. Gan, Y.-N. Xu, M.-Z. Huang, W.Y. Ching, and J.G. Harrison, Phys. Rev. B **45**, 8248 (1992); see also W.Y. Ching, F. Gan, and M.-Z. Huang, *ibid.* **52**, 1596 (1995).

[39] M. Catti, R. Dovesi, A. Pavese, and V.R. Saunders, J. Phys.: Condens. Matter **3**, 4151 (1991).

[40] R.A. Heaton and Ch.C. Lin, Phys. Rev. B **22**, 3629 (1980).

[41] J.P. Albert, C. Jouanin, and C. Gout, Phys. Rev. B **16**, 925 (1977).

[42] J. Barth, R.L. Johnson, M. Cardona, D. Fuchs, and A.M. Bradshaw, Phys. Rev. B **41**, 3291 (1990).

[43] K. Akai and M. Matsuura, Phys. Rev. B **60**, 5561 (1999).

[44] M. Verstraete and X. Gonze (unpublished).

[45] N. Troullier and J.L. Martins, Phys. Rev. B **43**, 1993 (1991).

[46] M. Mérawa, M. Llunell, R. Orlando, M. Gelize-Duvignau, and R. Dovesi, Chem. Phys. Lett. **368**, 7 (2003).

[47] R.W.G. Wyckoff, *Crystal Structures*, 2nd ed. (Wiley, New York, 1963), Vol. 1.
[48] A.A. Maradudin and A.E. Fein, Phys. Rev. **128**, 2589 (1962).
[49] For a review see, e.g., H. Bilz, D. Strauch, and R.K. Wehner, *Handbuch der Physik—Encyclopedia of Physics* (Springer, Berlin, 1984), Vol. 25/2d.
[50] G. Deinzer, G. Birner, and D. Strauch, Phys. Rev. B **67**, 144304 (2003).
[51] A. Debernardi, S. Baroni, and E. Molinari, Phys. Rev. Lett. **75**, 1819 (1995); A. Debernardi, Phys. Rev. B **57**, 12 847 (1998); A. Debernardi, C. Ulrich, K. Syassen, and M. Cardona, *ibid.* **59**, 6774 (1999).
[52] A. Debernardi and M. Cardona, Physica B **263–264**, 687 (1999); A. Debernardi, Solid State Commun. **113**, 1 (2000).
[53] R. Ruppin, J. Phys. Chem. Solids **33**, 83 (1972).
[54] R. Govindarajan, T.M. Haridasan, and J. Govindarajan, Phys. Status Solidi B **101**, 775 (1980).
[55] N. Dutt, A.J. Kaur, and J. Shanker, Phys. Status Solidi B **137**, 459 (1986).
[56] This approximation relies on the neglect of the frequency dependence of the damping and shift functions within the frequency regions of the spectral line.
[57] For larger anharmonicities and in a self-consistent phonon theory, one would need $\Gamma_{\lambda_0}(\Omega_0)$ at the anharmonically shifted frequency Ω_0.
[58] M.E. Lines, Phys. Rev. B **41**, 3372 (1990).